PHILOSOPHICAL TRANSACTIONS OF THE ROYAL SOCIETY A MATHEMATICAL, PHYSICAL & ENGINEERING SCIENCES

Bulk fluid phase behaviour of colloidal platelet–sphere and platelet–polymer mixtures

Daniel de las Heras and Matthias Schmidt

Phil. Trans. R. Soc. A 2013 **371**, 20120259, published 4 March 2013

PHILOSOPHICAL TRANSACTIONS OF THE ROYAL SOCIETY A

rsta.royalsocietypublishing.org

Research

Cite this article: de las Heras D, Schmidt M. 2013 Bulk fluid phase behaviour of colloidal platelet–sphere and platelet–polymer mixtures. Phil Trans R Soc A 371: 20120259. http://dx.doi.org/10.1098/rsta.2012.0259

One contribution of 14 to a Theo Murphy Meeting Issue 'New frontiers in anisotropic fluid–particle composites'.

Subject Areas:
statistical physics, chemical physics

Keywords:
colloids, phase transitions, nematic phase, discotic particles, colloid–polymer mixtures

Author for correspondence:
Daniel de Las Heras
e-mail: delasheras.daniel@gmail.com

Royal Society Publishing
Informing the science of the future

Bulk fluid phase behaviour of colloidal platelet–sphere and platelet–polymer mixtures

Daniel de las Heras and Matthias Schmidt

Theoretische Physik II, Physikalisches Institut, Universität Bayreuth, 95440 Bayreuth, Germany

Using a geometry-based fundamental measure density functional theory, we calculate bulk fluid phase diagrams of colloidal mixtures of vanishingly thin hard circular platelets and hard spheres. We find isotropic–nematic phase separation, with strong broadening of the biphasic region, upon increasing the pressure. In mixtures with large size ratio of platelet and sphere diameters, there is also demixing between two nematic phases with differing platelet concentrations. We formulate a fundamental measure density functional for mixtures of colloidal platelets and freely overlapping spheres, which represent ideal polymers, and use it to obtain phase diagrams. We find that, for low platelet–polymer size ratio, in addition to isotropic–nematic and nematic–nematic phase coexistence, platelet–polymer mixtures also display isotropic–isotropic demixing. By contrast, we do not find isotropic–isotropic demixing in hard-core platelet–sphere mixtures for the size ratios considered.

1. Introduction

Understanding the equilibrium properties of colloidal systems and the relationship between the microscopic properties, such as particle shapes and sizes, and the macroscopic properties of a dispersion is essential for the task of creating new materials with desired characteristics. Here, anisotropic colloids are relevant owing to the possible formation of liquid crystalline phases. Among them, platelet-like colloids are ubiquitous in nature; gibbsite or certain clays are specific examples.

Despite their simplicity, hard-core models are well-suited candidates to investigate the phase behaviour of colloidal systems. Since Onsager's [1] pioneering work on the isotropic–nematic (IN) phase transition in a fluid of rods, a wealth of studies have been carried out in order to elucidate the equilibrium properties of anisotropic

hard particles, including the fluid of circular platelets with vanishing thickness using Onsager-like theories [2,3] and fundamental measure theory (FMT) [4,5]; see Harnau [6] for a recent review of platelets and references [7–9] for reviews of FMT.

During the past few years, binary colloidal mixtures have received considerable attention. The addition of a second component induces profound changes in the phase diagram, with new phenomena arising such as demixing, reentrant phase boundaries, as well as the emergence of phase transitions due to the depletion mechanism. Studies of binary mixtures that involve platelets were conducted for mixtures of thick and thin platelets [10,11], binary platelets with different diameters [12] and mixtures of platelets and rods [13,14].

In this paper, we use density functional theory (DFT) [15], and in particular a geometry-based fundamental measure free energy functional [4], in order to investigate the bulk fluid properties in mixtures of infinitely thin platelets and hard spheres. Such mixtures have been previously considered by Harnau & Dietrich [16] using DFT and by Oversteegen & Lekkerkerker [17] by means of a free-volume scaled-particle approach. Those authors restricted their analyses to isotropic states of platelets. Both studies found coexistence between an isotropic fluid rich in platelets and a solid phase rich in spheres, as well as the stability of a phase transition between two isotropic phases with differing compositions for small values of the platelet–sphere size ratio. Both studies neglect the excluded-volume interaction between the platelets, which can certainly be a good approximation if the density of the platelets is very low. We will compare with these findings below. We compare also with results from an extended Onsager theory with Parsons–Lee rescaling [18,19] that includes two-body correlations only. By contrast, the geometry-based density functional that we use here includes explicitly non-local higher-body correlations. The non-local structure of the free energy functional [4] is specifically tailored for the present shapes. For general convex bodies, much recent effort [20–22] has been devoted to improve Rosenfeld's original FMT for non-spherical shapes [23–25].

Here, we also study mixtures of platelets and non-adsorbing ideal model polymers [26]. Polymers are modelled following the ideas of Asakura & Oosawa [27] and Vrij [28], i.e. they are treated as fully interpenetrable spheres that cannot overlap with the colloidal platelets. This is to be regarded only as a minimal model, in particular for the platelet–polymer interaction, as both softness and penetrability of a platelet into a polymer coil are neglected. We develop a fundamental measure DFT by linearizing the density functional for hard-core mixtures in polymer density [29,30].

Experimental mixtures of sterically stabilized gibbsite platelets and silica spheres have been studied very recently [31]. The authors found phase separation into platelet-rich and sphere-rich phases, driven by the repulsive interactions between particles of different species. Columnar ordering has been observed in charged mixtures of gibbsite platelets and silica spheres [32,33]. Furthermore, the crystallization of silica spheres in the presence of gibbsite platelets (silica-coated) was analysed by Oversteegen *et al*. [34].

The paper is organized as follows. In §2, we define the model and outline the DFT. The results are described in §3: mixtures of colloidal platelets and spheres are analysed in §3*a*; in §3*b*, we present the results for mixtures of colloidal platelets and ideal polymers; a comparison between FMT theory and an extended Onsager theory is given in §3*c*. Suggestions for future research lines and conclusions are presented in §4.

2. Model and theory

We consider a binary mixture of N_S hard spheres with radius R_S and N_D hard circular platelets with vanishing thickness and radius R_D; see figure 1 for a schematic illustration. Here and throughout, species-dependent quantities are indicated by subscripts S (spheres) and D (discs). The pair interaction potential between any two particles is infinite if the particles overlap, and vanishes otherwise.

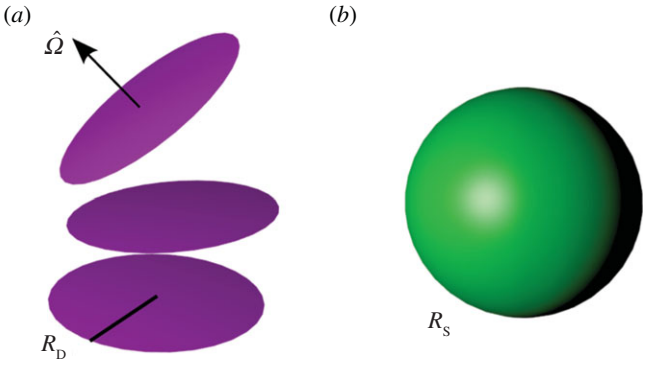

Figure 1. Schematic of the hard-core platelet–sphere mixture. The model is a binary mixture of (*a*) hard circular platelets of radius R_D with vanishing thickness and (*b*) hard spheres of radius R_S. The platelet orientation is described by a unit vector $\hat{\Omega}$ normal to the platelet surface. (Online version in colour.)

(a) Density functional theory for colloidal platelet–sphere mixtures

As is common, we split the Helmholtz free energy functional F into an ideal-gas part, F_{id}, and an excess contribution, F_{exc}. Hence

$$F = F_{id} + F_{exc}. \tag{2.1}$$

The ideal-gas free energy functional is exactly given by

$$\beta F_{id} = \int d^3r \int d\hat{\Omega}\, \rho_D(\boldsymbol{r}, \hat{\Omega})[\ln(\rho_D(\boldsymbol{r}, \hat{\Omega})\mathcal{V}_D) - 1] + \int d^3r \rho_S(\boldsymbol{r})[\ln(\rho_S(\boldsymbol{r})\mathcal{V}_S) - 1], \tag{2.2}$$

where $\beta = 1/k_BT$ is the inverse thermal energy, k_B is the Boltzmann constant, T is absolute temperature and $\mathcal{V}_i$ is the (irrelevant) thermal volume of species i. The spatial integral is over the system volume, V, and the angular integral is over the unit sphere; here, $\hat{\Omega}$ is a unit vector normal to the platelet surface (cf. figure 1). The one-body distribution function of platelets is denoted by $\rho_D(\boldsymbol{r}, \hat{\Omega})$, and that of spheres by $\rho_S(\boldsymbol{r})$, the latter being trivially independent of orientation owing to the rotational symmetry of the spheres. In general, both distribution functions depend on position $\boldsymbol{r}$. In the application to bulk fluid phase behaviour below, we consider only homogeneous states, which are independent of $\boldsymbol{r}$. Without loss of generality, we introduce an orientational distribution function for the platelets, $\Psi_D(\boldsymbol{r}, \hat{\Omega})$, via $\rho_D(\boldsymbol{r}, \hat{\Omega}) = \rho_D(\boldsymbol{r})\Psi_D(\boldsymbol{r}, \hat{\Omega})$. Here, $\rho_D(\boldsymbol{r})$ is the number density of platelets, which gives the differential number of platelets with any orientation in the differential volume element at $\boldsymbol{r}$.

The excess part of the free energy functional, F_{exc}, which accounts for the excluded-volume interactions between all particles, is approximated by a geometry-based density functional, which has the structure

$$\beta F_{exc} = \int d^3r\, \Phi(\{n_\nu^i\}), \tag{2.3}$$

where the reduced free energy density (Φ) is a function of a set of weighted densities, $\{n_\nu^i\}$, where $i = S, D$ labels the species, and ν the type of weight function. The free energy density can be grouped into three different contributions, $\Phi = \Phi_S + \Phi_D + \Phi_{SD}$. Here, Φ_S describes only sphere–sphere interactions. Both Φ_D and Φ_{SD} describe coupling of spheres and platelets, with Φ_D containing the terms that generate the FMT functional for pure platelets [4] in the limit of vanishing density of spheres. In detail, the reduced excess free energy for the interaction between spheres (Φ_S) is taken to be the original Rosenfeld form [23]

$$\Phi_S = -n_0^S \ln(1 - n_3^S) + \frac{n_1^S n_2^S - \boldsymbol{n}_{v1}^S \cdot \boldsymbol{n}_{v2}^S}{1 - n_3^S} + \frac{(n_2^S)^3 - 3n_2^S \boldsymbol{n}_{v2}^S \cdot \boldsymbol{n}_{v2}^S}{24\pi(1 - n_3^S)^2}. \tag{2.4}$$

Here and in the following two equations, we drop the spatial dependence on $\boldsymbol{r}$ of the weighted densities for the sake of notational convenience. The interactions between platelets are described by

$$\Phi_{\mathrm{D}} = \int \mathrm{d}\hat{\Omega}\, \frac{n_1^{\mathrm{DD}}(\hat{\Omega}) n_2^{\mathrm{D}}(\hat{\Omega})}{1-n_3^{\mathrm{S}}} + \int \mathrm{d}\hat{\Omega} \int \mathrm{d}\hat{\Omega}'\, \frac{n_2^{\mathrm{DDD}}(\hat{\Omega},\hat{\Omega}') n_2^{\mathrm{D}}(\hat{\Omega}) n_2^{\mathrm{D}}(\hat{\Omega}')}{24\pi(1-n_3^{\mathrm{S}})^2}. \tag{2.5}$$

The first term in equation (2.5) represents the interaction between two platelets. It reduces to the exact second-order contribution of the virial series for the free energy of platelets, if there are no spheres in the mixture ($\rho_{\mathrm{S}} = 0$). The second term corresponds to the interaction between three platelets (see [4,12] for details). The factors proportional to $(1 - n_3^{\mathrm{S}})$ in the denominators account for the volume occupied by the spheres in the system.

The further contribution to the reduced excess free energy due to the interaction between platelets and spheres is

$$\begin{aligned}\Phi_{\mathrm{SD}} = &- \int \mathrm{d}\hat{\Omega} n_0^{\mathrm{D}}(\hat{\Omega}) \ln(1-n_3^{\mathrm{S}}) + \int \mathrm{d}\hat{\Omega}\, \frac{n_1^{\mathrm{S}} n_2^{\mathrm{D}}(\hat{\Omega}) + n_2^{\mathrm{SD}}(\hat{\Omega}) n_1^{\mathrm{D}}(\hat{\Omega}) - \boldsymbol{n}_{v2}^{\mathrm{SD}}(\hat{\Omega}) \cdot \boldsymbol{n}_{v1}^{\mathrm{D}}(\hat{\Omega})}{1-n_3^{\mathrm{S}}} \\ &+ \int \mathrm{d}\hat{\Omega}\, \frac{[n_2^{\mathrm{SD}}(\hat{\Omega}) n_2^{\mathrm{SD}}(\hat{\Omega}) - \boldsymbol{n}_{v2}^{\mathrm{SD}}(\hat{\Omega}) \cdot \boldsymbol{n}_{v2}^{\mathrm{SD}}(\hat{\Omega})] n_2^{\mathrm{D}}(\hat{\Omega})}{8\pi(1-n_3^{\mathrm{S}})^2} \\ &+ \int \mathrm{d}\hat{\Omega} \int \mathrm{d}\hat{\Omega}'\, \frac{n_2^{\mathrm{SDD}}(\hat{\Omega},\hat{\Omega}') n_2^{\mathrm{D}}(\hat{\Omega}) n_2^{\mathrm{D}}(\hat{\Omega}')}{8\pi(1-n_3^{\mathrm{S}})^2}.\end{aligned} \tag{2.6}$$

All weighted densities are obtained by convolving the density with specific weight functions. For hard spheres, the scalar weighted densities are

$$n_\nu^{\mathrm{S}}(\boldsymbol{r}) = w_\nu^{\mathrm{S}}(\boldsymbol{r}) * \rho_{\mathrm{S}}(\boldsymbol{r}), \quad \nu = 0,1,2,3, \tag{2.7}$$

and the vectorial weighted densities are

$$\boldsymbol{n}_\nu^{\mathrm{S}}(\boldsymbol{r}) = \boldsymbol{w}_\nu^{\mathrm{S}}(\boldsymbol{r}) * \rho_{\mathrm{S}}(\boldsymbol{r}), \quad \nu = v1, v2, \tag{2.8}$$

where $*$ denotes the three-dimensional convolution $h(\boldsymbol{r}) * g(\boldsymbol{r}) = \int \mathrm{d}^3x\, h(\boldsymbol{x}) g(\boldsymbol{x}-\boldsymbol{r})$. Here, w_ν^{S} and $\boldsymbol{w}_\nu^{\mathrm{S}}$ are the Rosenfeld weight functions for hard spheres [23]:

$$\left.\begin{aligned} w_3^{\mathrm{S}}(\boldsymbol{r}) &= \Theta(R_{\mathrm{S}} - |\boldsymbol{r}|), \\ w_2^{\mathrm{S}}(\boldsymbol{r}) &= \delta(R_{\mathrm{S}} - |\boldsymbol{r}|) \\ \text{and} \qquad \boldsymbol{w}_{v2}^{\mathrm{S}}(\boldsymbol{r}) &= w_2^{\mathrm{S}}(\boldsymbol{r}) \frac{\boldsymbol{r}}{|\boldsymbol{r}|}, \end{aligned}\right\} \tag{2.9}$$

where $\Theta(\cdot)$ is the Heaviside step function and $\delta(\cdot)$ is Dirac's delta distribution. Further weight functions for hard spheres are $w_1^{\mathrm{S}}(\boldsymbol{r}) = w_2^{\mathrm{S}}(\boldsymbol{r})/(4\pi R_{\mathrm{S}})$, $w_0^{\mathrm{S}}(\boldsymbol{r}) = w_2^{\mathrm{S}}(\boldsymbol{r})/(4\pi R_{\mathrm{S}}^2)$ and $\boldsymbol{w}_{v1}^{\mathrm{S}}(\boldsymbol{r}) = \boldsymbol{w}_{v2}^{\mathrm{S}}(\boldsymbol{r})/(4\pi R_{\mathrm{S}})$.

The sphere–platelet coupling is described by the weighted densities

$$\left.\begin{aligned} n_2^{\mathrm{SD}}(\boldsymbol{r},\hat{\Omega}) &= w_2^{\mathrm{SD}}(\boldsymbol{r},\hat{\Omega}) * \rho_{\mathrm{S}}(\boldsymbol{r}), \\ \boldsymbol{n}_{v2}^{\mathrm{SD}}(\boldsymbol{r},\hat{\Omega}) &= \boldsymbol{w}_{v2}^{\mathrm{SD}}(\boldsymbol{r},\hat{\Omega}) * \rho_{\mathrm{S}}(\boldsymbol{r}) \\ \text{and} \qquad n_2^{\mathrm{SDD}}(\boldsymbol{r},\hat{\Omega},\hat{\Omega}') &= w_2^{\mathrm{SDD}}(\boldsymbol{r},\hat{\Omega},\hat{\Omega}') * \rho_{\mathrm{S}}(\boldsymbol{r}), \end{aligned}\right\} \tag{2.10}$$

where the weight functions are

$$\left.\begin{aligned} w_2^{\mathrm{SD}}(\boldsymbol{r},\hat{\Omega}) &= \frac{4}{\pi}\sqrt{1-(\boldsymbol{r}\cdot\hat{\Omega}/R_{\mathrm{S}})^2}\, w_2^{\mathrm{S}}(\boldsymbol{r}), \\ \boldsymbol{w}_{v2}^{\mathrm{SD}}(\boldsymbol{r},\hat{\Omega}) &= 4\frac{\boldsymbol{r}-(\boldsymbol{r}\cdot\hat{\Omega})\hat{\Omega}}{\pi R_{\mathrm{S}}} w_2^{\mathrm{S}}(\boldsymbol{r}) \\ \text{and} \qquad w_2^{\mathrm{SDD}}(\boldsymbol{r},\hat{\Omega},\hat{\Omega}') &= \frac{8}{\pi}|(\hat{\Omega}\times\hat{\Omega}')\cdot\boldsymbol{w}_{v2}^{\mathrm{S}}(\boldsymbol{r})|. \end{aligned}\right\} \tag{2.11}$$

Finally, the weighted densities for platelets are

$$\left.\begin{aligned} n_\nu^{\mathrm{D}}(\boldsymbol{r},\hat{\Omega}) &= w_\nu^{\mathrm{D}}(\boldsymbol{r},\hat{\Omega}) * \rho_{\mathrm{D}}(\boldsymbol{r},\hat{\Omega}), \quad \nu = 0,1,2,\\ \boldsymbol{n}_{\upsilon 1}^{\mathrm{D}}(\boldsymbol{r},\hat{\Omega}) &= \boldsymbol{w}_{\upsilon 1}^{\mathrm{D}}(\boldsymbol{r},\hat{\Omega}) * \rho_{\mathrm{D}}(\boldsymbol{r},\hat{\Omega}),\\ n_1^{\mathrm{DD}}(\boldsymbol{r},\hat{\Omega}') &= \int \mathrm{d}\hat{\Omega} w_1^{\mathrm{DD}}(\boldsymbol{r},\hat{\Omega},\hat{\Omega}') * \rho_{\mathrm{D}}(\boldsymbol{r},\hat{\Omega})\\ \text{and}\qquad n_2^{\mathrm{DDD}}(\boldsymbol{r},\hat{\Omega},\hat{\Omega}') &= \int \mathrm{d}\hat{\Omega}'' w_2^{\mathrm{DDD}}(\boldsymbol{r},\hat{\Omega}'',\hat{\Omega},\hat{\Omega}') * \rho_{\mathrm{D}}(\boldsymbol{r},\hat{\Omega}''), \end{aligned}\right\} \tag{2.12}$$

and their corresponding weight functions are

$$\left.\begin{aligned} w_0^{\mathrm{D}}(\boldsymbol{r},\hat{\Omega}) &= \frac{1}{2\pi R_{\mathrm{D}}}\delta(R_{\mathrm{D}} - |\boldsymbol{r}|)\delta(\boldsymbol{r}\cdot\hat{\Omega}),\\ w_1^{\mathrm{D}}(\boldsymbol{r},\hat{\Omega}) &= \frac{1}{8}\delta(R_{\mathrm{D}} - |\boldsymbol{r}|)\delta(\boldsymbol{r}\cdot\hat{\Omega}),\\ \boldsymbol{w}_{\upsilon 1}^{\mathrm{D}}(\boldsymbol{r},\hat{\Omega}) &= \frac{\boldsymbol{r}}{R_{\mathrm{D}}} w_1^{\mathrm{D}}(\boldsymbol{r},\hat{\Omega}),\\ w_2^{\mathrm{D}}(\boldsymbol{r},\hat{\Omega}) &= 2\Theta(R_{\mathrm{D}} - |\boldsymbol{r}|)\delta(\boldsymbol{r}\cdot\hat{\Omega}),\\ w_1^{\mathrm{DD}}(\boldsymbol{r},\hat{\Omega},\hat{\Omega}') &= \frac{2}{R_{\mathrm{D}}}\left|\hat{\Omega}\cdot(\hat{\Omega}'\times\boldsymbol{r})\right| w_1^{\mathrm{D}}(\boldsymbol{r},\hat{\Omega})\\ \text{and}\qquad w_2^{\mathrm{DDD}}(\boldsymbol{r},\hat{\Omega},\hat{\Omega}',\hat{\Omega}'') &= \frac{8}{\pi}\left|\hat{\Omega}\cdot(\hat{\Omega}'\times\hat{\Omega}'')\right| w_2^{\mathrm{D}}(\boldsymbol{r},\hat{\Omega}). \end{aligned}\right\} \tag{2.13}$$

The density functional described here is a special case of the functional for ternary platelet–sphere–needle mixtures [4]. It includes contributions up to third order in platelet density. It reduces to the original Rosenfeld functional [23] in the case of a monodisperse fluid of hard spheres, and gives results that are in good agreement with Monte Carlo simulation data when describing a monodisperse fluid of vanishingly thin platelets [4,12,35]. Hence, we are confident that it can be applied successfully to the study of binary mixtures of hard spheres and platelets.

(b) Density functional theory for mixtures of colloidal platelets and ideal polymers

We use a model [26] similar in spirit to the colloid–polymer model of Asakura & Oosawa [27] and Vrij [28] (AOV), to study a mixture of colloidal platelets, which are, as above, taken as infinitely thin circular discs, and ideal polymers. The polymers are modelled by fully interpenetrable spheres of radius R_{P}. These model polymers cannot overlap with the platelets. We obtain an approximation for the free energy of this system by linearizing the excess part of the free energy for the corresponding hard-core system. This strategy follows the derivation of the FMT for the AOV model from a corresponding binary hard-sphere mixture [29,30]. Hence, we apply the linearization to the hard-core functional of §3*a* in order to obtain a free energy functional for the polymer–platelet mixture, $F_{\mathrm{exc}}^{\mathrm{PD}}$, via

$$F_{\mathrm{exc}}^{\mathrm{PD}}[\rho_{\mathrm{D}},\rho_{\mathrm{P}}] = F_{\mathrm{exc}}[\rho_{\mathrm{D}},\rho_{\mathrm{S}}=0] + \int \mathrm{d}^3 r \left.\frac{\delta F_{\mathrm{exc}}}{\delta\rho_{\mathrm{S}}(\boldsymbol{r})}\right|_{\rho_{\mathrm{S}}=0} \rho_{\mathrm{P}}(\boldsymbol{r}), \tag{2.14}$$

where $\rho_{\mathrm{P}}(\boldsymbol{r})$ is the one-body polymer density distribution, and F_{exc} is the free energy functional for the hard-core mixture, given in equation (2.3). $F_{\mathrm{exc}}^{\mathrm{PD}}$ can be expressed in terms of a reduced free energy density

$$\beta F_{\mathrm{exc}}^{\mathrm{PD}} = \int \mathrm{d}^3 r\, \Phi_{\mathrm{PD}}(\{n_\nu^i\}), \tag{2.15}$$

where the reduced free energy, Φ_{PD}, is a simple expression linear in polymer density and with up to cubic contributions in platelet density:

$$\begin{aligned}\Phi_{\mathrm{PD}} = &\int \mathrm{d}\hat{\Omega} n_0^{\mathrm{D}}(\hat{\Omega}) n_3^{\mathrm{P}}(\hat{\Omega}) + \int \mathrm{d}\hat{\Omega} (n_1^{\mathrm{P}}(\hat{\Omega}) n_2^{\mathrm{D}}(\hat{\Omega}) + n_2^{\mathrm{PD}}(\hat{\Omega}) n_1^{\mathrm{D}}(\hat{\Omega}) - \boldsymbol{n}_{v2}^{\mathrm{PD}}(\hat{\Omega}) \cdot \boldsymbol{n}_{v1}^{\mathrm{D}}(\hat{\Omega}))\\ &+ \int \mathrm{d}\hat{\Omega} \int \mathrm{d}\hat{\Omega}' \frac{n_2^{\mathrm{PDD}}(\hat{\Omega}, \hat{\Omega}') n_2^{\mathrm{D}}(\hat{\Omega}) n_2^{\mathrm{D}}(\hat{\Omega}')}{8\pi} + \int \mathrm{d}\hat{\Omega} n_1^{\mathrm{DD}}(\hat{\Omega}) n_2^{\mathrm{D}}(\hat{\Omega})(1 + n_3^{\mathrm{P}})\\ &+ \int \mathrm{d}\hat{\Omega} \int \mathrm{d}\hat{\Omega}' \frac{n_2^{\mathrm{DDD}}(\hat{\Omega}, \hat{\Omega}') n_2^{\mathrm{D}}(\hat{\Omega}) n_2^{\mathrm{D}}(\hat{\Omega}')}{24\pi} (1 + 2n_3^{\mathrm{P}}). \end{aligned} \tag{2.16}$$

We have suppressed the spatial dependence of the weighted densities in the above expressions. The weighted densities that depend on the polymer density (denoted by the letter P in the superscript) are those for hard spheres (2.7) and (2.8), but replacing the hard-sphere colloid density, $\rho_{\mathrm{S}}(\boldsymbol{r})$, by the polymer density, $\rho_{\mathrm{P}}(\boldsymbol{r})$, and replacing the colloid radius, R_{C}, by the polymer radius, R_{P}.

(c) Spatially homogeneous fluids

In the following, we restrict ourselves to considering spatially homogeneous fluid states. We use the sphere–platelet model (the expressions for the polymer–platelet model being analogous). The density distributions are independent of the spatial coordinates and

$$\left.\begin{aligned} &\rho_{\mathrm{S}}(\boldsymbol{r}) = \rho_{\mathrm{S}} = \text{const}\\ \text{and}\quad &\rho_{\mathrm{D}}(\boldsymbol{r}, \hat{\Omega}) = \rho_{\mathrm{D}} \Psi_{\mathrm{D}}(\hat{\Omega}), \quad \text{where } \rho_{\mathrm{D}} = \text{const.} \end{aligned}\right\} \tag{2.17}$$

The total number of spheres (N_{S}) and that of platelets (N_{D}) are obtained by integrating the number densities over the system volume:

$$\left.\begin{aligned} N_{\mathrm{S}} &= \int \mathrm{d}^3 r \rho_{\mathrm{S}},\\ \text{and}\quad N_{\mathrm{D}} &= \int \mathrm{d}^3 r \rho_{\mathrm{D}}. \end{aligned}\right\} \tag{2.18}$$

Equation (2.18) implies that the orientational distribution function of platelets is normalized according to

$$\int \mathrm{d}\hat{\Omega} \Psi_{\mathrm{D}}(\hat{\Omega}) = 1, \tag{2.19}$$

which is a different convention compared to that of Esztermann *et al.* [4]. As we do not expect biaxial arrangements of the platelets to occur in bulk, we take the orientational distribution function to depend only on the polar angle θ with respect to the nematic director, hence $\Psi(\hat{\Omega}) = \Psi(\theta)$. We use a parameter, Λ, and prescribe the functional form of the orientational distribution function as

$$\Psi_{\mathrm{D}}(\theta) = \frac{\exp[\Lambda \mathrm{P}_2(\cos\theta)]}{\int \mathrm{d}\hat{\Omega} \exp[\Lambda \mathrm{P}_2(\cos\theta)]}, \tag{2.20}$$

satisfying by construction the normalization condition (2.19). Here, $\mathrm{P}_2(\cdot)$ is the second Legendre polynomial, and Λ determines the degree of orientational order of the platelets. For isotropic states, $\Psi_{\mathrm{D}}(\theta) = 1/4\pi$ is obtained for $\Lambda = 0$. We characterize the orientational order of the platelets by S_{D}, the standard nematic order parameter:

$$S_{\mathrm{D}} = \int \mathrm{d}\hat{\Omega} \Psi_{\mathrm{D}}(\theta) \mathrm{P}_2(\cos\theta). \tag{2.21}$$

We have tested the quality of the parametrization (2.20) by computing the isotropic–nematic (IN) phase transition of the monodisperse fluid of platelets, and comparing the coexisting densities and order parameter with those obtained from free minimization [4]. The differences for the coexistence densities between the two methods are of the order of 1 per cent; see table 1 for a

Table 1. Coexistence values for the IN phase transition of a monodisperse fluid of hard circular platelets with vanishing thickness. The values in the first row are from free minimization without an *a priori* form of the orientational distribution function [12]. The second row shows the coexisting values using the parametrization (2.20). Monte Carlo data [36] are presented in the third row. In the fourth row, the results from Onsager theory are shown; these are identical to Parsons–Lee theory (§2*d*), as the packing fraction vanishes in the pure system of platelets. Here, $\rho_{\mathrm{D}}^{\mathrm{I}}$ and $\rho_{\mathrm{D}}^{\mathrm{N}}$ are the coexistence densities at the IN transition, and $S_{\mathrm{D}}^{\mathrm{N}}$ is the nematic order parameter in the coexisting nematic state.

$\Psi_{\mathrm{D}}(\theta)$	$\rho_{\mathrm{D}}^{\mathrm{I}} R_{\mathrm{D}}^3$	$\rho_{\mathrm{D}}^{\mathrm{N}} R_{\mathrm{D}}^3$	$S_{\mathrm{D}}^{\mathrm{N}}$
FMT, free minimization [12]	0.419	0.469	0.533
FMT, parametrization (2.20)	0.421	0.462	0.489
Monte Carlo [36]	0.460	0.498	0.45–0.55
Onsager theory	0.672	0.858	0.801

comparison. The value of the nematic order parameter at coexistence, S_{D}^{N}, deviates more strongly from the result of free minimization. However, as its magnitude is unusually small for the pure platelet system, this is a very sensitive quantity; see the discussion in Phillips & Schmidt [12]. For completeness, table 1 also gives the results from Onsager theory and from Monte Carlo simulations.

In spatially homogeneous fluids, the weighted densities are obtained by integrating the weight functions over the spatial coordinates. For hard spheres, we have

$$\left.\begin{aligned} n_0^{\mathrm{S}} &= \rho_{\mathrm{S}}, \\ n_1^{\mathrm{S}} &= R_{\mathrm{S}}\rho_{\mathrm{S}}, \\ n_2^{\mathrm{S}} &= 4\pi R_{\mathrm{S}}^2\rho_{\mathrm{S}}, \\ n_3^{\mathrm{S}} &= \tfrac{4}{3}\pi R_{\mathrm{S}}^3\rho_{\mathrm{S}} \end{aligned}\right\} \tag{2.22}$$

and

$$\boldsymbol{n}_{v1}^{\mathrm{S}} = \boldsymbol{n}_{v2}^{\mathrm{S}} = 0.$$

The mixed weighted densities that couple spheres and platelets are

$$\left.\begin{aligned} n_2^{\mathrm{SD}}(\hat{\Omega}) &= 4\pi R_{\mathrm{S}}^2\rho_{\mathrm{S}}, \\ n_{v2}^{\mathrm{SD}}(\hat{\Omega}) &= 0 \end{aligned}\right\} \tag{2.23}$$

and

$$n_2^{\mathrm{SDD}}(\theta,\theta') = \rho_{\mathrm{S}}\int_{-R_{\mathrm{S}}}^{R_{\mathrm{S}}} \mathrm{d}z \int_0^{2\pi} \mathrm{d}\phi' \begin{cases} 32\pi\,|t|, & \text{if } t^2 > s^2, \\ 64\left(\sqrt{s^2-t^2} + t\arcsin\dfrac{t}{s}\right), & \text{otherwise,} \end{cases} \tag{2.24}$$

where $t = z\sin\theta\sin\theta'\sin\phi'$, and

$$s = \sqrt{R_{\mathrm{S}}^2 - z^2}\sqrt{\sin^2\theta\cos^2\theta' + \cos^2\theta\sin^2\theta' - 2\sin\theta\cos\theta\sin\theta'\cos\theta'\cos\phi'}. \tag{2.25}$$

Owing to our normalization (2.19), equation (2.24) and equation (105) of Esztermann *et al*. [4] differ by a factor $(4\pi)^2$. The integrals over the azimuthal angles ϕ and ϕ' have been performed in order to arrive at (2.24), as only the polar angle with respect to the nematic director is relevant for uniaxial configurations.

For platelets, the bulk weight functions reduce to

$$\left.\begin{aligned} n_0^{\mathrm{D}}(\hat{\Omega}) &= \rho_{\mathrm{D}}\Psi_{\mathrm{D}}(\hat{\Omega}), \\ n_1^{\mathrm{D}}(\hat{\Omega}) &= \frac{\pi}{4}R_{\mathrm{D}}\rho_{\mathrm{D}}\Psi_{\mathrm{D}}(\hat{\Omega}), \\ n_2^{\mathrm{D}}(\hat{\Omega}) &= 2\pi R_{\mathrm{D}}^2\rho_{\mathrm{D}}\Psi_{\mathrm{D}}(\hat{\Omega}) \end{aligned}\right\} \tag{2.26}$$

and

$$\boldsymbol{n}_{v1}^{\mathrm{D}}(\hat{\Omega}) = 0.$$

Further contributions to the free energy due to the weighted densities n_1^{DD} and n_2^{DDD} are the same as given in equations (13) and (27) of Phillips & Schmidt [12], to which we refer the reader directly.

The angular integrals were calculated numerically using Gaussian quadrature. We used 2000 roots for the integrals over the azimuthal angle and 25 roots for the integrals in the polar angle. The orientational distribution function does not depend on the azimuthal angle, and hence the integrals over ϕ can be computed and stored for subsequent use. We checked the accuracy of the numerical procedure by computing selected coexisting points with 100 roots for the integrals over the polar angle. The differences were less than 1 per cent.

(d) Parsons–Lee theory for colloidal platelet–sphere mixtures

Parsons–Lee theory [18,19] constitutes an approximation where the second virial contribution to the excess free energy is weighted with a prefactor in order to approximate the effects of higher virial contributions. According to Parsons–Lee theory, the excess free energy for a spatially homogeneous binary mixture of hard bodies can be written as [37]

$$\frac{\beta F_{\mathrm{exc}}}{V} = \phi(\eta) \sum_{ij} \rho_i \rho_j \int \mathrm{d}\hat{\Omega} \int \mathrm{d}\hat{\Omega}' \Psi_i(\hat{\Omega}) \Psi_j(\hat{\Omega}') v_{\mathrm{ex}}^{ij}(\Omega, \Omega'), \tag{2.27}$$

where $v_{\mathrm{ex}}^{ij}(\hat{\Omega}, \hat{\Omega}')$ is the excluded volume between two particles of species i and j with orientations given by $\hat{\Omega}$ and $\hat{\Omega}'$, respectively. The prefactor $\phi(\eta)$ depends on the chosen reference system. Here, η is the total packing fraction of the mixture, $\eta = \sum_i \rho_i v_i$, where v_i is the particle volume of species i. Our reference system is a pure fluid of hard spheres, and for the present model $\eta = v_{\mathrm{S}} \rho_{\mathrm{S}}$, as the platelet volume vanishes. Using the Carnahan–Starling equation of state, the prefactor in the excess free energy is

$$\phi(\eta) = \frac{4 - 3\eta}{8(1-\eta)^2}. \tag{2.28}$$

The orientational distribution function for spheres is $\Psi_{\mathrm{S}}(\hat{\Omega}) = 1/4\pi$, and for platelets is given in equation (2.20). The excluded volume between two spheres is

$$v_{\mathrm{ex}}^{\mathrm{SS}}(\hat{\Omega}, \hat{\Omega}') = \tfrac{32}{3} \pi R_{\mathrm{S}}^3, \tag{2.29}$$

between platelets and spheres is

$$v_{\mathrm{ex}}^{\mathrm{DS}}(\hat{\Omega}, \hat{\Omega}') = 2\pi R_{\mathrm{S}} R_{\mathrm{D}}^2 + \pi^2 R_{\mathrm{D}} R_{\mathrm{S}}^2 + \tfrac{4}{3} \pi R_{\mathrm{S}}^3, \tag{2.30}$$

and, finally, between two platelets is

$$v_{\mathrm{ex}}^{\mathrm{DD}}(\hat{\Omega}, \hat{\Omega}') = 4\pi R_{\mathrm{D}}^3 \sin\gamma, \tag{2.31}$$

where γ is the angle between $\hat{\Omega}$ and $\hat{\Omega}'$. For pure platelets $\eta = 0$, and hence (2.28) reduces to $\phi(\eta) = \frac{1}{2}$, which renders (2.27) identical to the (Onsager) second virial functional.

(e) Coexistence conditions

In what follows, we denote the composition of the mixture, x, by the molar fraction of hard spheres, i.e. $x = \rho_{\mathrm{S}}/\rho$, where $\rho = \rho_{\mathrm{S}} + \rho_{\mathrm{D}}$ is the total density. The molar fraction of platelets is then simply $\rho_{\mathrm{D}}/\rho = 1 - x$. The equilibrium properties of the mixture are obtained by minimizing the Gibbs free energy per particle $g = F/N_{\mathrm{T}} + p/\rho$ at constant composition x, pressure p and temperature T. Here, F is the total Helmholtz free energy, and $N_{\mathrm{T}} = N_{\mathrm{S}} + N_{\mathrm{D}}$ is the total number of particles. We use a standard Newton–Raphson method to minimize g as a function of ρ and Λ. Binodal lines are located by a common-tangent construction on $g(x)$, which is equivalent to the equality of chemical potentials of both species at the coexisting values of x and ρ. Thermal and mechanical equilibrium are satisfied in advance by fixing both temperature and pressure.

Correspondingly, for the platelet–polymer mixture, $x = \rho_P/\rho$ and $\rho = \rho_P + \rho_D$. The coexistence conditions are those given earlier, with colloidal sphere quantities exchanged by the respective polymer quantities.

3. Results

The pure fluid of hard platelets with vanishing thickness undergoes a first-order IN phase transition as a function of density. Table 1 summarizes the values for the coexisting densities and for the nematic order parameter according to the present FMT. The results are in good agreement with Monte Carlo simulation data [38,39]. Columnar and solid phases appear only in the limit of infinite density in a pure system of platelets with vanishing thickness [36]. In a monodisperse fluid of hard spheres, there is a well-known first-order fluid–solid phase transition on increasing the density. We have not studied spatially ordered phases, but give some comments about the stability of spatially homogeneous phases with respect to hard-sphere crystallization in §4.

(a) Mixtures of colloidal platelets and spheres

In figure 2, we present the phase behaviour of mixtures of platelets and spheres for three different mixtures with size ratios $R_D/R_S = 2$ (figure 2*a–c*(i)), 5 (figure 2*a–c*(ii)) and 10 (figure 2*a–c*(iii)). We comment on the behaviour for smaller size ratios at the end of the section. In figure 2*a*(i), we show the phase diagram in the plane of reduced pressure, $\beta p R_D^3$, and molar fraction of spheres, x, for a mixture with size ratio $R_D/R_S = 2$. The IN phase transition in the pure fluid of platelets ($x = 0$) moves to higher pressures and the fractionation becomes stronger when spheres are added to the system. Upon increasing the pressure, the nematic branch of the binodal initially moves to higher compositions, but then bends back on itself approaching $x = 0$. The nematic phase is stable only when the molar fraction for spheres is very low.

In figure 2*b*(i), we plot the phase diagram for the same mixture in the plane of reduced density of discs, $\rho_D R_D^3$, and packing fraction of spheres, $\rho_S v_S$, where v_S is the sphere volume. The IN biphasic region strongly broadens when the packing fraction of spheres in the mixture is increased. The orientational order parameter of platelets, S_D, along the nematic side of the binodal is shown in figure 2*c*(i). We also display the total orientational order parameter of the mixture, i.e. the nematic order parameter of platelets weighted by the composition of platelets,

$$S_{tot} = \frac{\rho_D}{\rho S_D} = (1 - x) S_D. \tag{3.1}$$

As the composition of spheres at the IN phase transition is low, the two orientational order parameters are similar to each other, increasing along the nematic side of the binodal.

The second column of figure 2 shows the results for mixtures with $R_D/R_S = 5$, i.e. for increased relative size of the platelets. The topology of the phase diagrams in both representations is the same as in the above mixture. The main difference to the case of $R_D/R_S = 2$ is the strongly increased range of compositions for which the nematic phase is stable. For example, in figure 2*a*(ii) one can observe that, for a range of pressures, it is possible to find a stable nematic phase even if the composition of the mixture is $x \gtrsim 0.6$. The mechanism that induces the IN phase transition is different at low and at high pressures. At low pressures, the transition is mainly due to the gain in configurational entropy of the platelets in the nematic phase, as the excluded volume between two platelets is minimal if they are parallel to each other. In this regime, there is low partitioning between the isotropic and nematic phases. At high pressures, however, the transition is driven by the (unfavourable) excluded-volume interactions between platelets and spheres. As a result, there is strong demixing between a nematic phase rich in platelets and an isotropic phase mostly composed of spheres.

We focus next on the behaviour of ρ_D along the nematic branch of the binodal. For low size ratios, it monotonically increases as spheres are added to the mixture; but for $R_D/R_S \gtrsim 2$, ρ_D slightly decreases when the packing fraction of spheres is low (see the inset of figure 2*b*(ii)). This

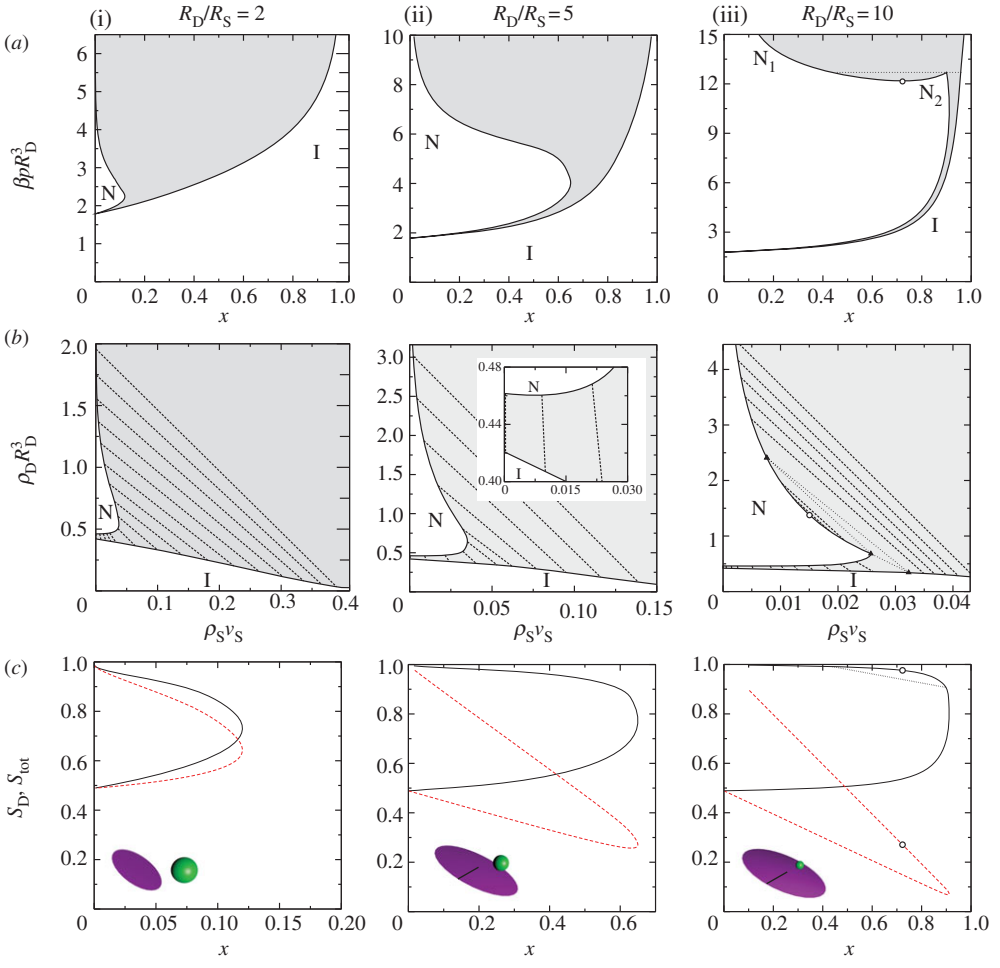

Figure 2. Phase diagrams of binary mixtures of spheres and platelets with three different values of the platelet–sphere size ratio: $R_D/R_S = 2$ (i), 5 (ii) and 10 (iii). For each mixture, we show (*a*) the reduced pressure $\beta p R_D^3$ versus composition of spheres x, (*b*) the reduced density of platelets $\rho_D R_D^3$ as a function of the packing fraction for spheres $\rho_S v_S$ and (*c*) the nematic order parameters along the nematic side of the binodal. The shaded areas indicate two-phase regions. Empty circles represent critical points. Dotted lines represent triple points. The dashed lines in the second row are selected tie lines that connect two coexisting points on the binodal. The inset in (*b*(ii)) is a zoom of the region close to the IN phase transition of the pure fluid of platelets. The solid black (dashed red) lines in the third row represent the platelets' (total) nematic order parameter, S_D (S_T). The insets in the third row are cartoons showing the relative size between species. (Online version in colour.)

behaviour appears to be counter-intuitive. However, a reduction in the density of platelets at which the nematic phase is stable in the mixture has recently been observed in sedimentation experiments on sterically stabilized mixtures of gibbsite platelets and silica spheres [31] of size ratio ≈ 6. However, the authors found a much stronger effect than that obtained in our theory. The quantitative difference could be due to the influence of gravity on the bulk phase diagram [40]. The polydispersity of the components, the finite thickness of the platelets and further interactions between the particles (not purely entropic, as we are considering here) in the experimental set-up could also be relevant to explain the quantitative differences.

The last column in figure 2 shows results for the phase behaviour of a mixture with size ratio $R_D/R_S = 10$. A prominent alteration of the topology of the phase diagram is that, in addition to the IN phase transition, there is also demixing between two nematic phases with differing

compositions. The nematic–nematic phase coexistence region is bounded by a lower critical point and merges with the IN phase transition at an isotropic–nematic–nematic triple point. At pressures above the triple point pressure, there is strong demixing between an isotropic phase rich in spheres and a nematic phase mostly composed of platelets. The nematic–nematic demixing can be viewed as being driven by a depletion attraction induced between the platelets by the small spheres.

The behaviour of the orientational order parameters along the binodal is shown in the third row of figure 2. For small size ratios, figure 2*c*(i), both the order parameter of platelets, S_D, and the total order parameter, S_{tot}, increase along the nematic branch of the binodal. However, in mixtures where the size ratio is high (figure 2*c*(ii), (iii)), S_D monotonically increases along the binodal, but the total order parameter, S_{tot}, first decreases to a minimum and then increases. This qualitative difference may be observable experimentally.

The phase diagrams of mixtures with size ratios $R_D/R_S < 2$ (not shown) are qualitatively similar to the results for $R_D/R_S = 2$. In particular, the topology remains unchanged and only IN phase separation occurs. This is in contrast to previous studies of mixtures of infinitely thin platelets and hard spheres [16,17], which reported isotropic–isotropic demixing if the size ratio of the mixture is small. In our DFT treatment, we do not find isotropic–isotropic coexistence in the range of size ratios $0.2 \leq R_D/R_S \leq 10$.

(b) Mixtures of colloidal platelets and ideal polymers

We turn to the analysis of mixtures of colloidal platelets and ideal model polymers. Bates and Frenkel studied such mixtures using Monte Carlo simulations and perturbation theory [26]. Following the ideas of Asakura and Oosawa [27] and Vrij [28], the polymers are modelled as freely interpenetrable spheres that cannot overlap with the platelets due to the hard repulsion between the unlike species. A DFT for such mixture is obtained by linearizing the excess free energy, equation (2.3), around $\rho_S = 0$ (see §2*b* for details).

The bulk fluid phase behaviour of mixtures of colloidal platelets and non-adsorbing polymers is depicted in figure 3 for three different values of the size ratio R_D/R_P. The upper row shows the phase diagram in the pressure–composition plane. The polymer fugacity, $z_P = \exp(\beta\mu_P)/\mathcal{V}_P$, with μ_P the chemical potential of the polymers, as a function of the density of platelets is represented in the lower row. Here, the chemical potential of species i is obtained from $\partial F/\partial N_i = \mu_i$. Note that the fugacity is independent of the (hence irrelevant) thermal volume $\mathcal{V}_P$ because the chemical potential μ_p is shifted according to the particular choice of $\mathcal{V}_P$.

The main difference to platelet–colloid mixtures is that mixtures of platelets and ideal polymers display prominent demixing between two isotropic states when the size ratio is low enough. In figure 3*a*(i), we show the results for $R_D/R_P = 2$. There is strong demixing between two isotropic phases bounded by a lower critical point. The isotropic–isotropic phase separation occurs almost entirely at pressures below the IN pressure of the pure fluid of platelets. At higher pressures, the isotropic–isotropic binodal merges with the IN binodal via a nematic–isotropic–isotropic triple point. This phase diagram differs significantly from that of the hard-core mixture with the same size ratio shown in figure 2*a*(i). The difference between the two systems lies in the sphere–sphere excluded-volume interactions. In a mixture of platelets and ideal polymers, the gain in accessible volume in the demixed isotropic–isotropic state overcompensates the loss of mixing entropy. This is not the case in mixtures of colloidal platelets and spheres for the size ratios considered. It is interesting to note that isotropic–isotropic demixing has been found by computer simulation in mixtures of platelets with finite thickness and non-adsorbing polymers [41].

In figure 3*b*(i), we show a comparison with Monte Carlo simulation data (full circles) [26] for the same mixture ($R_D/R_P = 2$). The agreement is reasonably good, although DFT underestimates the IN coexisting densities at low polymer concentration and also the fugacity of the polymers along both branches of the isotropic–isotropic binodal and hence the location of the critical point. This trend is similar to what was found for the AOV model [42].

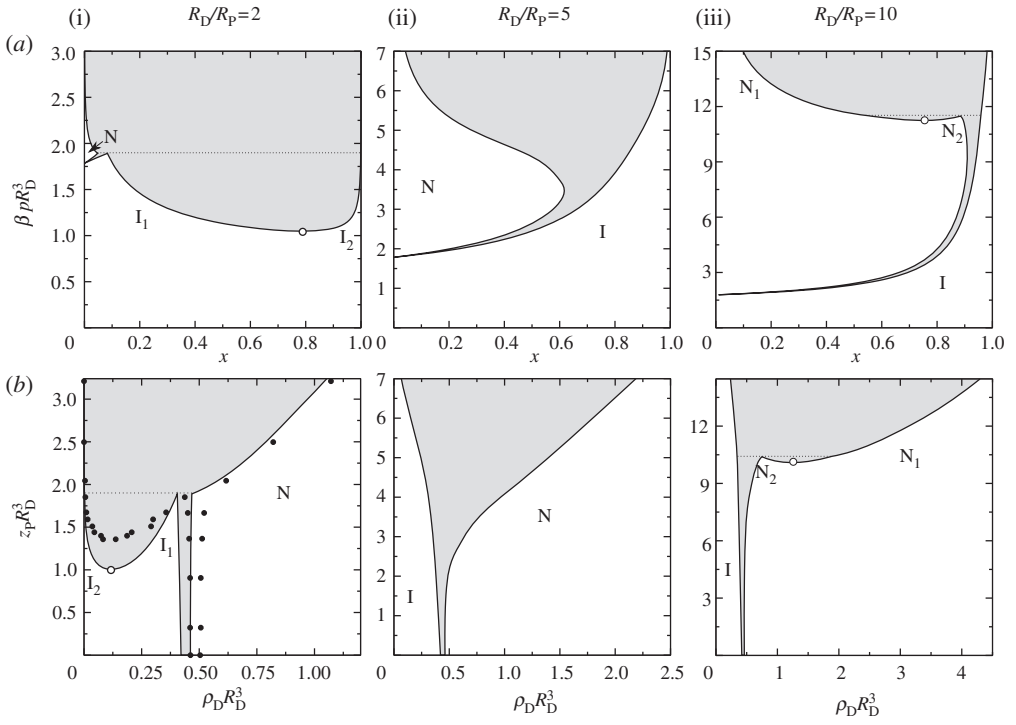

Figure 3. Phase diagrams of mixtures of colloidal platelets and ideal model polymers for size ratios $R_D/R_P = 2$ (i), 5 (ii) and 10 (iii). For each mixture, we show (*a*) pressure, $\beta p R_D^3$, as a function of the composition of polymers, x, and (*b*) fugacity of the polymers, $z_P R_D^3$, versus density of platelets, $\rho_D R_D^3$. Empty circles represent critical points. Dotted lines represent triple points. Full circles in (*b*(i)) indicate Monte Carlo simulation data [26].

The middle (right) column of figure 3 shows the phase diagrams of a mixture with size ratio $R_D/R_P = 5$ ($R_D/R_P = 10$). The behaviour is very similar to the corresponding mixtures of colloidal spheres and platelets, depicted in figure 2*a*(ii), (iii). Such similarity might be expected because, by increasing the relative size of the platelets (in hard-core platelet–sphere mixtures), the platelet–platelet and platelet–sphere interactions dominate over the sphere–sphere interactions. Recall that we do not consider the freezing transition of hard spheres, which would dramatically change the phase behaviour between ideal polymers and colloidal spheres at densities above the freezing transition.

Our results are in qualitative agreement with the experimental observations. For example, isotropic–isotropic coexistence has been found in suspensions of sterically stabilized colloidal gibbsite platelets and non-adsorbing polymers (with $R_D/R_P \approx 2.9$) by Lekkerkerker *et al.* [43]. The same study also showed a strong broadening of the IN two-phase region on increasing the polymer concentration. Nematic–nematic demixing has recently been found [44] in a related system of mixtures of non-adsorbing polymers and positively charged platelets.

(c) Fundamental measure theory versus Parsons–Lee theory

The geometry-based DFT of §2*a* contains contributions to the excess free energy that are of third order in density. In this section, we compare the results from this theory to those from an extended Onsager theory with Parsons–Lee rescaling that explicitly includes only two-body interactions. For details about Parsons–Lee theory, see §2*d*. The phase diagram of a hard-core mixture with size ratio $R_D/R_S = 2$ according to Parsons–Lee theory is depicted in figure 4. It is to be compared with figure 2*a*,*b*(i), where corresponding results obtained from FMT are shown. An immediately noticeable difference is in the location of the IN phase transition in the pure fluid of platelets. In

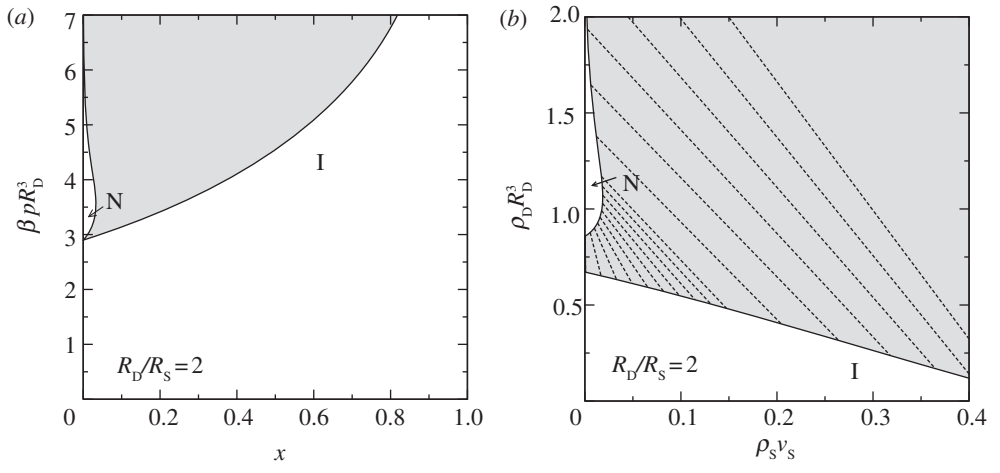

Figure 4. Bulk phase diagrams of a colloidal mixture of platelets and spheres according to Parsons–Lee theory. (*a*) Scaled pressure $\beta p R_D^3$ versus composition of spheres x. (*b*) Density of platelets $\rho_D R_D^3$ as a function of the packing fraction of spheres $\rho_S v_S$. The size ratio is $R_D/R_S = 2$.

this limit ($x = 0$), Parsons–Lee theory gives an unchanged result when compared with Onsager theory owing to the vanishing packing fraction in the pure fluid of platelets. Hence, Parsons–Lee theory clearly overestimates the coexisting densities ($\rho_D^I R_D^3 = 0.67$ and $\rho_D^N R_D^3 = 0.86$). It also predicts a much too high nematic order parameter at the IN coexistence, $S_N = 0.80$ (not shown), compared with FMT and Monte Carlo simulation.

For $R_D/R_S = 2$, the topology of the phase diagram predicted by the two theories is the same. According to Parsons–Lee theory, the partitioning between isotropic and nematic phases is higher than in FMT. A similar trend was observed on comparing the current FMT and Onsager theory in binary mixtures of hard platelets with different radius [12]. Parsons–Lee theory predicts demixing between two nematic phases in mixtures with high size ratio, as does FMT. However, the minimal size ratio for phase segregation to occur between two nematics using Parsons–Lee theory is $R_D/R_S \gtrsim 15$, considerably higher than the threshold for FMT, which is $R_D/R_S \approx 10$. One important difference is that Parsons–Lee theory predicts isotropic–isotropic demixing for low size ratios $R_D/R_S \lesssim 1$. Nevertheless, the isotropic–isotropic phase boundary is located at very high pressures and densities, and is most probably metastable with respect to segregation between an isotropic phase rich in platelets and a solid phase rich in spheres.

4. Conclusions

We have investigated the fluid bulk phase behaviour of mixtures of colloidal platelets and spheres using a geometry-based DFT [4]. The size ratio R_D/R_S is the key parameter that controls the behaviour of the system. In mixtures with $0.2 \leq R_D/R_S \lesssim 10$, we find only IN phase separation. We have identified two different mechanisms behind the IN phase transition. If the composition of spheres is low, the IN transition is driven by the excluded-volume interaction between the platelets, similar to the mechanism in a pure fluid of platelets. In this regime, the transition takes place between two phases with low partitioning. As the composition of spheres is increased, the interaction between dissimilar species becomes dominant, and the (unfavourable) excluded-volume interactions between spheres and platelets drives strong demixing between an isotropic sphere-rich phase and a nematic platelet-rich phase.

Mixtures with high size ratio, $R_D/R_S \gtrsim 10$, also display demixing between two nematics at different compositions. However, reliably describing such highly asymmetric mixtures is very difficult for any theoretical treatment; see the comparison of FMT and simulation results for asymmetric binary hard-sphere mixtures [45,46].

The possible existence of demixing between two isotropic fluids in mixtures of colloidal platelets and spheres remains an open question. The FMT approach does not predict isotropic–isotropic demixing. Previous studies [16,17] reported isotropic–isotropic phase separation in mixtures where the size of both species is similar. Nevertheless, in both studies, the authors neglected excluded-volume interactions between platelets. This approximation is valid only if the platelet density is very low. By contrast, our theory includes platelet–platelet interactions, modelled via up to cubic contributions in platelet density to the free energy. The bulk free energy for isotropic states from the present DFT is the same as that from scaled-particle theory [47], which gives further confidence in our results. Carrying out a careful simulation study in order to shed further light on the existence of isotropic–isotropic demixing in the hard-core mixture would be very valuable.

We have not considered spatially inhomogeneous phases in this work. The pure fluid of hard spheres undergoes a fluid–solid phase transition. The freezing transition, according to Monte Carlo simulations [48,49], takes place at packing fractions $\rho_S v_S = 0.49$ for the liquid and 0.54 for the solid (values that are higher than the packing fractions considered in the present work). Hence, we expect our fluid phase diagrams to be stable with respect to freezing of the hard spheres. For low size ratios (smaller than those analysed here), we expect an isotropic–solid demixing region in the phase diagram. Columnar as well as solid phases become relevant in the systems of platelets with non-vanishing thickness at sufficiently high densities. Hence, it is possible that nematic–nematic demixing in mixtures with high size ratio will be metastable with respect to columnar ordering. Recent experiments by Lekkerkerker and co-workers on mixtures of charged gibbsite platelets and silica spheres [32,33] have shown a large isotropic–columnar coexisting region. Columnar ordering has also been studied theoretically in mixtures of board-like platelets and spheres in a cubic lattice [50]. Smectic phases are not very common in discotic liquid crystals, but they could appear in real systems with finite thickness [51]. Recent experiments with mixtures of colloidal gibbsite platelets and spheres [52] show that also glass formation can occur at sufficiently high sphere concentrations.

As our theory is mean-field in character, we expect the location of the nematic–nematic critical point to change upon including neglected fluctuations, say in computer simulations. Such (future) work could ascertain the stability of nematic–nematic demixing. Furthermore, it would be interesting to consider the stability of the nematic–nematic transition upon altering the platelet–polymer interactions, in order to take into account penetrability of platelets and polymers.

The results presented in this work can form the basis for studies of inhomogeneous platelet–sphere mixtures using DFT, such as the analysis of gravity [40,53], as well as wetting and confinement effects.

References

1. Onsager L. 1949 The effects of shape on the interaction of colloidal particles. *Ann. NY Acad. Sci.* **51**, 627–659. (doi:10.1111/j.1749-6632.1949.tb27296.x)
2. Forsyth PA, Marcelja S, Mitchell DJ, Ninham BW. 1977 Onsager transition in hard plate fluid. *J. Chem. Soc. Faraday Trans. 2* **73**, 84–88. (doi:10.1039/F29777300084)
3. Forsyth PA, Marcelja S, Mitchell DJ, Ninham BW. 1978 Ordering in colloidal systems. *Adv. Colloid Interface Sci.* **9**, 7–60. (doi:10.1016/0001-8686(87)80002-7)
4. Esztermann A, Reich H, Schmidt M. 2006. Density functional theory for colloidal mixtures of hard platelets, rods, and spheres. *Phys. Rev. E* **73**, 011409. (doi:10.1103/PhysRevE.73.011409)
5. Reich H, Schmidt M. 2007 Capillary nematization of hard colloidal platelets confined between two parallel hard walls. *J. Phys. Condensed Matter* **19**, 326103. (doi:10.1088/0953-8984/19/32/326103)
6. Harnau L. 2008 Structure and thermodynamics of platelet dispersions. *Mol. Phys.* **106**, 1975–2000. (doi:10.1080/00268970802032301)
7. Roth R. 2010 Fundamental measure theory for hard-sphere mixtures: a review. *J. Phys. Condensed Matter* **22**, 063102. (doi:10.1088/0953-8984/22/6/063102)

8. Tarazona P, Cuesta JA, Martinez-Raton Y. 2008 Density functional theories of hard particle systems. In *Theory and simulation of hard-sphere fluids and related systems* (ed. A Mulero). Lecture Notes in Physics, vol. 753, pp. 247–341. Berlin, Germany: Springer. (doi:10.1007/978-3-540-78767-9_7)
9. Lutsko JF. 2010 Recent developments in classical density functional theory. In *Advances in chemical physics* (ed. SA Rice), vol. 144, pp. 1–92. Hoboken, NJ: John Wiley. (doi:10.1002/9780470564318.ch1)
10. Wensink HH, Vroege GJ, Lekkerkerker HNW. 2001 Isotropic–nematic density inversion in a binary mixture of thin and thick hard platelets. *J. Phys. Chem. B* **105**, 10 610–10 618. (doi:10.1021/jp0105894)
11. Wensink HH, Vroege GJ. 2004 Demixing in binary mixtures of anisometric colloids. *J. Phys. Condensed Matter* **16**, S2015–S2027. (doi:10.1088/0953-8984/16/19/013)
12. Phillips J, Schmidt M. 2010 Bulk phase behavior of binary hard platelet mixtures from density functional theory. *Phys. Rev. E* **81**, 041401. (doi:10.1103/PhysRevE.81.041401)
13. Varga S, Galindo A, Jackson G. 2002 Global fluid phase behavior in binary mixtures of rodlike and platelike molecules. *J. Chem. Phys.* **117**, 7207–7221. (doi:10.1063/1.1507112)
14. Berardi R, Zannoni C. 2012 Low-temperature biaxial nematic from rod and disc mesogen mixture. *Soft Matter* **8**, 2017–2025. (doi:10.1039/C1SM06838E)
15. Evans R. 1979 The nature of the liquid–vapour interface and other topics in the statistical mechanics of non-uniform, classical fluids. *Adv. Phys.* **28**, 143–200. (doi:10.1080/00018737900101365)
16. Harnau L, Dietrich S. 2005 Bulk and wetting phenomena in a colloidal mixture of hard spheres and platelets. *Phys. Rev. E* **71**, 011504. (doi:10.1103/PhysRevE.71.011504)
17. Oversteegen SM, Lekkerkerker HNW. 2004 Phase diagram of mixtures of hard colloidal spheres and discs: a free-volume scaled-particle approach. *J. Chem. Phys.* **120**, 2470–2474. (doi:10.1063/1.1637573)
18. Parsons JD. 1979 Nematic ordering in a system of rods. *Phys. Rev. A* **19**, 1225–1230. (doi:10.1103/PhysRevA.19.1225)
19. Lee S. 1987 A numerical investigation of nematic ordering based on a simple hard-rod model. *J. Chem. Phys.* **87**, 4972–4974. (doi:10.1063/1.452811)
20. Hansen-Goos H, Mecke K. 2009 Fundamental measure theory for inhomogeneous fluids of nonspherical hard particles. *Phys. Rev. Lett.* **102**, 018302. (doi:10.1103/PhysRevLett.102.018302)
21. Korden S. 2012. Deriving the Rosenfeld functional from the virial expansion. *Phys. Rev. E* **85**, 041150. (doi:10.1103/PhysRevE.85.041150)
22. Korden S. 2012. Beyond the Rosenfeld functional: loop contributions in fundamental measure theory. (http://arxiv.org/abs/1208.3932)
23. Rosenfeld Y. 1989 Free-energy model for the inhomogeneous hard-sphere fluid mixture and density-functional theory of freezing. *Phys. Rev. Lett.* **63**, 980–983. (doi:10.1103/PhysRevLett.63.980)
24. Rosenfeld Y. 1994 Density functional theory of molecular fluids: free-energy model for the inhomogeneous hard-body fluid. *Phys. Rev. E* **50**, R3318–R3321. (doi:10.1103/PhysRevE.50.R3318)
25. Rosenfeld Y. 1995 Free energy model for the inhomogeneous hard-body fluid: application of the Gauss–Bonnet theorem. *Mol. Phys.* **86**, 637–647. (doi:10.1080/00268979500102241)
26. Bates MA, Frenkel D. 2000 Phase behavior of model mixtures of colloidal disks and polymers. *Phys. Rev. E* **62**, 5225–5229. (doi:10.1103/PhysRevE.62.5225)
27. Oosawa F, Asakura S. 1954 Surface tension of high-polymer solutions. *J. Chem. Phys.* **22**, 1255–1255. (doi:10.1063/1.1740346)
28. Vrij A. 1976 Polymers at interfaces and the interactions in colloidal dispersions. *Pure Appl. Chem.* **48**, 471–483. (doi:10.1351/pac197648040471)
29. Schmidt M, Löwen H, Brader JM, Evans R. 2000 Density functional for a model colloid–polymer mixture. *Phys. Rev. Lett.* **85**, 1934–1937. (doi:10.1103/PhysRevLett.85.1934)
30. Schmidt M, Löwen H, Brader JM, Evans R. 2002 Density functional theory for a model colloid–polymer mixture: bulk fluid phases. *J. Phys. Condensed Matter* **14**, 9353–9382. (doi:10.1088/0953-8984/14/40/323)
31. Doshi N, Cinacchi G, van Duijneveldt JS, Cosgrove T, Prescott SW, Grillo I, Phipps J, Gittins DI. 2011 Structure of colloidal sphere–plate mixtures. *J. Phys. Condensed Matter* **23**, 194109. (doi:10.1088/0953-8984/23/19/194109)

32. Kleshchanok D, Meijer JM, Petukhov AV, Portale G, Lekkerkerker HNW. 2012 Sedimentation and depletion attraction directing glass and liquid crystal formation in aqueous platelet/sphere mixtures. *Soft Matter* **8**, 191–197. (doi:10.1039/C1SM06535A)
33. Kleshchanok D, Meijer JM, Petukhov AV, Portale G, Lekkerkerker HNW. 2010 Structures and phase behavior in mixtures of charged colloidal spheres and platelets. *Langmuir* **26**, 13 614–13 621. (doi:10.1021/la101891e)
34. Oversteegen SM, Vonk C, Wijnhoven JEGJ, Lekkerkerker HNW. 2005 Crystallization in settling mixtures of colloidal spheres and plates. *Phys. Rev. E* **71**, 041406. (doi:10.1103/PhysRevE.71.041406)
35. Cheung DL, Anton L, Allen MP, Masters AJ, Phillips J, Schmidt M. 2008 Structure and stability of isotropic states of hard platelet fluids. *Phys. Rev. E* **78**, 041201. (doi:10.1103/PhysRevE.78.041201)
36. Bates MA, Frenkel D. 1998 Infinitely thin disks exhibit a first order nematic–columnar phase transition. *Phys. Rev. E* **57**, 4824–4826. (doi:10.1103/PhysRevE.57.4824)
37. Cinacchi G, Martínez-Ratón Y, Mederos L, Velasco E. 2006 Smectic, nematic, and isotropic phases in binary mixtures of thin and thick hard spherocylinders. *J. Chem. Phys.* **124**, 234904. (doi:10.1063/1.2207141)
38. Marechal M, Cuetos A, Martínez-Haya B, Dijkstra M. 2011 Phase behavior of hard colloidal platelets using free energy calculations. *J. Chem. Phys.* **134**, 094501. (doi:10.1063/1.3552951)
39. Frenkel D, Eppenga R. 1982 Monte Carlo study of the isotropic–nematic transition in a fluid of thin hard disks. *Phys. Rev. Lett.* **49**, 1089–1092. (doi:10.1103/PhysRevLett.49.1089)
40. de las Heras D, Doshi N, Cosgrove T, Phipps J, Gittins DI, van Duijneveldt JS, Schmidt M. 2012 Floating nematic phase in colloidal platelet–sphere mixtures. *Sci. Rep.* **2**, 789. (doi:10.1038/srep00789)
41. Zhang S, Reynolds PA, van Duijneveldt JS. 2002 Phase behavior of mixtures of colloidal platelets and nonadsorbing polymers. *J. Chem. Phys.* **117**, 9947–9958. (doi:10.1063/1.1518007)
42. Vink RLC, Horbach J. 2004 Grand canonical Monte Carlo simulation of a model colloid–polymer mixture: coexistence line, critical behavior, and interfacial tension. *J. Chem. Phys.* **121**, 3253–3258. (doi:10.1063/1.1773771)
43. van der Kooij FM, Vogel M, Lekkerkerker HNW. 2000 Phase behavior of a mixture of platelike colloids and nonadsorbing polymer. *Phys. Rev. E* **62**, 5397–5402. (doi:10.1103/PhysRevE.62.5397)
44. Cousin F, Cabuil V, Grillo I, Levitz P. 2008 Competition between entropy and electrostatic interactions in a binary colloidal mixture of spheres and platelets. *Langmuir* **24**, 11 422–11 430. (doi:10.1021/la8015595)
45. Herring AR, Henderson JR. 2006 Simulation test of hard-body colloidal physics. *Phys. Rev. Lett.* **97**, 148302. (doi:10.1103/PhysRevLett.97.148302)
46. Ashton DJ, Wilding NB, Roth R, Evans R. 2011 Depletion potentials in highly size-asymmetric binary hard-sphere mixtures: comparison of simulation results with theory. *Phys. Rev. E* **84**, 061136. (doi:10.1103/PhysRevE.84.061136)
47. Barker JA, Henderson D. 1976 What is 'liquid'? Understanding the states of matter. *Rev. Mod. Phys.* **48**, 587–671. (doi:10.1103/RevModPhys.48.587)
48. Vega C, Noya EG. 2007 Revisiting the Frenkel–Ladd method to compute the free energy of solids: the Einstein molecule approach. *J. Chem. Phys.* **127**, 154113. (doi:10.1063/1.2790426)
49. Fortini A, Dijkstra M. 2006 Phase behaviour of hard spheres confined between parallel hard plates: manipulation of colloidal crystal structures by confinement. *J. Phys. Condensed Matter* **18**, L371–L378. (doi:10.1088/0953-8984/18/28/L02)
50. Peroukidis SD, Vanakaras AG, Photinos DJ. 2010 Liquid crystalline phases and demixing in binary mixtures of shape-anisometric colloids. *J. Mater. Chem.* **20**, 10 495–10 502. (doi:10.1039/C0JM01692F)
51. Sun D, Sue H, Cheng Z, Martinez-Ratón Y, Velasco E. 2009 Stable smectic phase in suspensions of polydisperse colloidal platelets with identical thickness. *Phys. Rev. E* **80**, 041704. (doi:10.1103/PhysRevE.80.041704)
52. Kleshchanok D, Meijer JM, Petukhov AV, Portale G, Lekkerkerker HNW. 2011 Attractive glass formation in aqueous mixtures of colloidal gibbsite platelets and silica spheres. *Soft Matter* **7**, 2832–2840. (doi:10.1039/C0SM01206H)
53. Wensink HH, Lekkerkerker HNW. 2004 Sedimentation and multi-phase equilibria in mixtures of platelets and ideal polymer. *Europhys. Lett.* **66**, 125. (doi:10.1209/epl/i2003-10140-1)